

Mesoscopic Modeling for Continua with Pores: Application in Biological Soft Tissue

Kerstin Weinberg^{*} and Thomas Böhme

Institut für Mechanik, Lehrstuhl Kontinuumsmechanik und Materialtheorie
(LKM), Sekr. MS-2, Technische Universität Berlin, Einsteinufer 5, 10587
Berlin, Germany

^{*}Corresponding author (kerstin.weinberg@tu-berlin.de)

Communicated by K.H. Hoffmann, Chemnitz, Germany, and
C.A. Papenfuss, Berlin, Germany

Abstract

In this work, the damage in biological soft tissue induced by bubble cavitation is investigated. A typical medical procedure with such damaging side effects is the kidney stone fragmentation by shock-wave lithotripsy. We start with a mesoscopic continuum model that allows the consideration of microstructural information within the macroscopic balance equations. An evolution equation for the temporal development of the bubble distribution function is derived. Furthermore, the constitutive relations of bubble expansion are deduced by means of a spherical shell model. Numerical simulations are presented for a typical soft tissue material and different definitions for a damage parameter are discussed.

1. Introduction

Biological soft tissue such as, human skin, the eye's cornea, fat or kidney tissue, are by nature complex composite materials. The mechanical modeling of such materials is – even in a very simplified and homogenized way – open to considerable debate. Neither the microstructural description of millions of (different) cells nor the complete negligence of microscopic effects is an option. The situation becomes even more complicated in the presence of damaging mechanisms.

An example for a classical medical procedure with damaging side effects on soft tissue is the noninvasive comminution of kidney stones. The idea of such an extracorporeal shock wave lithotripsy (ESWL) treatment is to generate a

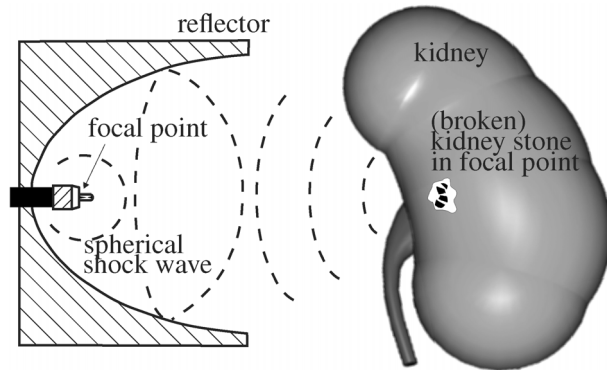


Figure 1 Shock wave-induced destruction of kidney stones.

number of high-intensity pressure waves (shock waves) outside the patient and to fire them onto the stone within the kidney, cf. Figure 1. The urologist controls the number of shock waves administered (typically 1000–3000), the repetition rate (typically one per second), and the voltage (or energy) of the shock wave generator. The latter is directly associated with the amplitude of the pressure wave. Thus, by shock wave reflection, spallation, and erosion, the stone gets fragmented into pieces, which can be passed the natural way.

ESWL therapy was developed over twenty years ago, and has proven to be fast, effective, and relatively free from the trauma and expense associated with surgery. However, although effective in breaking kidney stones, ESWL can also cause significant short- and long-term damage to the kidneys. The extent of kidney injuries depends on many factors, such as the size of the kidney, blood pressure, the age of the patient, etc., but meanwhile it is established knowledge that adverse effects can be observed on both cellular and systemic levels. A likely reason for this is cellular wall rupture (lysis) induced by shearing and cavitation. Cavitation, a phenomenon well known from shock-wave subjected fluids, means the generation of empty or gas-filled bubbles that oscillate up to macroscopic size. During bubble expansion, the surrounding vessels and capillaries dilate and may rupture. This mechanism causes irreversible changes within the kidney tissue material.

In order to capture such effects, we present here a mesoscopic theory for a general solid material with a certain time- and load-dependent damage evolution. We model the material to be in its virgin state homogenous and isotropic and to develop a microstructure as a consequence of mechanical loading. The simplifying assumptions for the reference state are justified, e.g., for the kidney, by the irregular and non uniformly textured tissue. The specific phenomenon of cavitation induced oscillating bubbles is modelled here as an evolution of spherical pores within the soft tissue.

The general mesoscopic concept was introduced by Muschik and his co-workers [1–3] in order to model microstructural effects within a continuum mechanical framework. Part of this concept is the introduction of a statistical function describing the microstructural distribution; in our case, this is the arrangement of bubbles or pores. The particular advantage of such a mesoscopic approach is the possibility to derive damage parameters as a macroscopic measure of microscopic changes.

The remaining of the paper is organized as follows: In the next section we first describe the underlying model of a porous soft tissue, and in Section 3 we provide the basic equations of the mesoscopic framework. The actual constitutive model of bubble growth in an elastic material is outlined in Section 4, together with the discussion of two possible damage parameters for injured soft tissue. We briefly summarize the results and discuss some open questions in Section 5.

2. General model of a soft tissue with pores

2.1. Spherical shell model

The majority of natural and technical materials contains a certain amount of arbitrarily distributed pores and cavities. Typically, the cavities are small compared to the size of the structure; their spatial average over the current volume of the body V defines the pore volume fraction or porosity $f_V(t)$. The initial porosity of the materials under consideration here is presumed to be low, e.g., $10^{-4} - 10^{-2}$. Contrary to classical engineering materials, biological soft tissues show little resistance to hydrostatic tension; under straining, the pores may grow until surrounding cell walls and capillaries rupture.

In order to analyze the growth of cavities and pores in a deforming material, we imagine that *each* pore i with volume $V_{\text{pore}}^{(i)}$ is at every instance completely embedded in the material (matrix). In other words, we exclude here the process of coalescence. The shell of material with volume $V_{\text{shell}}^{(i)}$ embedding the pore is surrounded by a surface $S^{(i)}$ lying wholly in the material; cf. Figure 2 (lower right). For every pore i it holds

$$\frac{V_{\text{pore}}^{(i)}}{V} = f_V^{(i)} \quad \text{and} \quad \sum_i V_{\text{shell}}^{(i)} = V - V_{\text{rem}}, \quad (1)$$

where V denotes the total volume and V_{rem} is the remaining volume left between the surfaces $S^{(i)}$. The fraction of remaining volume, V_{rem}/V , is presumed to be known. In the following, we assume, for simplicity, this volume

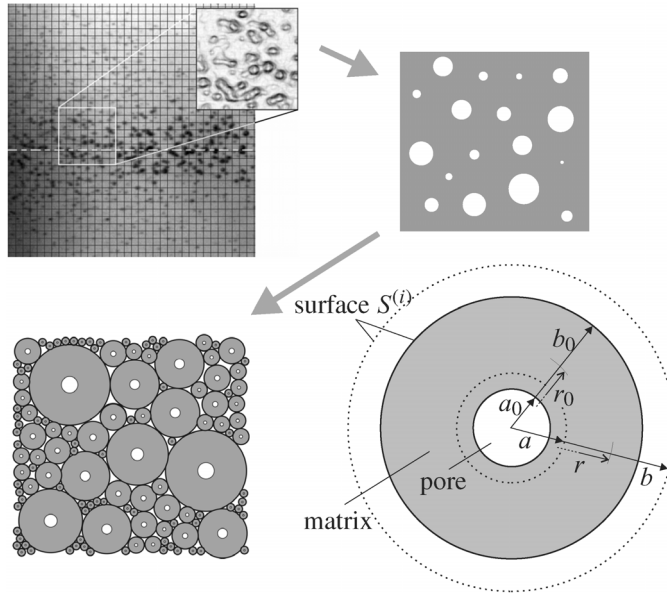


Figure 2. Spherical shell model of a porous soft tissue motivated by experimental observations of [4], and a spherical shell model of one single pore before and after (dashed lines) deformation.

to vanish $V_{\text{rem}} \rightarrow 0$. For a moderate porosity (up to $1/3$), a subdivision of the material could be carried out and we assume that this has been done in such a way that the surfaces $S^{(i)}$ approach spheres as nearly as possible. Therefore, in the following any element containing a pore will be called a **spherical shell**.

The porous material is now modeled as assemblages of such spherical shells; cf. Figure 2 (lower left). A material like this may be thought of as “constructed” by filling a body with spherical shells which are diminished to infinitesimal size. In its virgin state, i.e., at time $t = 0$, the pore volume fraction of each spherical shell, $f_{V0}^{(i)}$, equals the (low) overall porosity. We presume the initial porosity as well as the initial pore size distribution to be known for a representative volume at given position \mathbf{x} .

As a consequence of mechanical or thermal loading, the representative volume may expand and the spherical shells may grow in different ways but retain their shapes (no overlapping). As the remaining volume between the spheres can be infinitesimally small, the deformation energy density of the porous material will in the limit approach the sum of deformation energy densities stored in all spherical shells.

2.2. Kinematics of pore growth

Let us consider one spherical shell with initial inner radius a_0 and outer radius b_0 and let it expand for some reason toward current radii $a \equiv a(t)$ and $b \equiv b(t)$, respectively; cf. Figure 2 (lower right). Pore and shell volume then specify to $V_{\text{pore}}^{(i)} = 4\pi/3 a^3$ and $V_{\text{shell}}^{(i)} = 4\pi/3 b^3$. Moreover, presuming a volume preserving deformation, it holds

$$\frac{d}{dt} (V_{\text{shell}}^{(i)} - V_{\text{pore}}^{(i)}) = 0. \quad (2)$$

Consider now a material sphere surrounding the pore and deforming with the body. The initial and current radii of that material sphere are denoted by $r_0 \in [a_0, b_0]$ and $r \equiv r(t) \in [a, b]$, respectively. With volume constraint (2), the deformation mapping $r = \varphi(r_0)$ is uniquely determined by

$$\frac{4\pi}{3}(r^3 - a^3) = \frac{4\pi}{3}(r_0^3 - a_0^3) \quad \Rightarrow \quad r = (r_0^3 - a_0^3 + a^3)^{1/3}. \quad (3)$$

As a consequence, the current outer radius of a shell of incompressible material surrounding a pore is given by $b(a) = (b_0^3 - a_0^3 + a^3)^{1/3}$, and all subsequent equations depending on the shell radius b can be expressed in terms of the pore radius a and the initial geometry.

Writing the volume constraint (2) equivalently as

$$\frac{d}{dt} \frac{4\pi}{3} (r^3 - a^3) = 0$$

defines the velocity field over the current configuration. In particular, the spatial velocity field and its radial component at spatial position \mathbf{x} are

$$v_r = \frac{dr}{dt} = \frac{a^2}{r^2} \dot{a} \quad \text{and} \quad \mathbf{v} = \frac{v_r}{r} \mathbf{x} = \frac{a^2 \dot{a}}{r^3} \mathbf{x}, \quad (4)$$

where the rate of pore radius, $\dot{a}(t)$, is the velocity of pore expansion,

$$\frac{da}{dt} \equiv \dot{a}(a, t).$$

In view of the soft biological tissues considered here, the pores in the material are actually provoked by (expanding) bubbles. Therefore, we will later refer to $\dot{a}(a, t)$ simply as **bubble velocity**.

3. A modicum of the mesoscopic concept

3.1. General balance equations

The balance equations of classical continuum physics are defined on the *configurational space* $\mathbb{R} \times \mathbb{R}^3$ spanned by time $t \in \mathbb{R}$ and the position $\mathbf{x} \in \mathbb{R}^3$ of a set of particles¹ \mathcal{P} occupying a region $\Omega \subset \mathbb{R}^3$. Considering standard materials, the *five wanted fields* of mass density $\varrho(\mathbf{x}, t)$, material velocity $\mathbf{v}(\mathbf{x}, t)$, and specific (total) energy $e(\mathbf{x}, t)$ are determined by the universal, i.e., material-independent, balance equation of mass, momentum, and energy. In order to specify the balances for certain materials, additional equations for the material quantities, such as (Cauchy) stress tensor $\boldsymbol{\sigma}$ or heat flux density \mathbf{q} , must be inserted. These so-called *constitutive* relations, whose domain defines the *state space*, must satisfy the entropy inequality and close up the balances to a system of partial differential equations (PDE) solvable by means of initial and boundary conditions.

Let us consider a domain $\Omega(t)$ exchanging heat, power, and material with its environment, which is commonly defined to be a Schottky system; see Figure 3 (left). The temporal change of an extensive quantity $\Psi(\mathbf{x}, t)$ in the system can only be invoked by a production Π^Ψ within the volume, by a supply Σ^Ψ , and by a flux \mathbf{J}^Ψ of quantity Ψ over the boundaries of the volume. Thus, the *generic form* of a *global balance equation* reads for continuous fields

$$\begin{aligned} \frac{d\Psi}{dt} &= \frac{d}{dt} \int_{\Omega(t)} \rho \psi(\mathbf{x}, t) dV = \\ &= - \int_{\partial\Omega(t)} \mathbf{J}^\Psi(\mathbf{x}, t) \cdot \mathbf{n} dS + \int_{\Omega(t)} (\Pi^\Psi(\mathbf{x}, t) + \Sigma^\Psi(\mathbf{x}, t)) dV, \quad (5) \end{aligned}$$

where ψ identifies the (mass-)specific quantity of $\Psi(\mathbf{x}, t)$ and \mathbf{n} the (outward) normal vector on the surface $S \equiv \partial\Omega$.

If $\Omega(t)$ always contains the same particles, the system is called a body, a system of bodies, or a *closed system*. In this case, there is no particle transfer over the boundary $\partial\Omega$, i.e., the total mass remains constant:

$$\frac{d}{dt} \int_{\Omega(t)} \rho(\mathbf{x}, t) dV = 0 \quad (\text{global mass balance for closed systems}). \quad (6)$$

Obviously, Eq. (6) represents a special case of Eq. (5) with $\psi \equiv 1$, $\mathbf{J}^\Psi = \Pi^\Psi = \Sigma^\Psi \equiv 0$. On the other hand, a Schottky system may be modelled as an

¹For brevity, we label the material particles $\mathcal{P} \in \Omega$ by their position vectors $\mathbf{x}(\mathcal{P})$ in a certain reference placement and relative to some coordinate system $\mathbf{x} = x^i \mathbf{g}_i$.

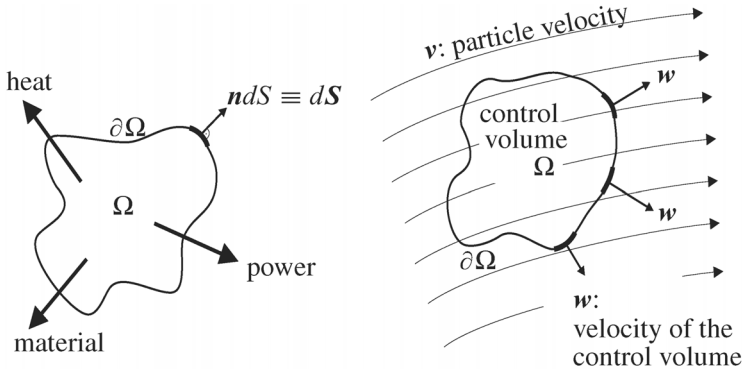


Figure 3. Definition of a Schottky system Ω with boundary $\partial\Omega$, velocity \mathbf{w} and particle velocity \mathbf{v} .

open system presuming a constant control volume moving with velocity \mathbf{w} ; see Figure 3 (right). Note that the velocity \mathbf{w} is superposed to the material velocity $\mathbf{v}(\mathbf{x}, t)$ of the particles \mathcal{P} . Then it holds for the flux of mass $\mathbf{J}^\psi \equiv \mathbf{J}^1 = \mathbf{J}$, and one can notify the *global mass balance of an open system*:

$$\frac{d}{dt} \int_{\Omega(t)} \rho(\mathbf{x}, t) dV = - \int_{\partial\Omega(t)} \mathbf{J}(\mathbf{x}, t) \cdot \mathbf{n} dS \neq 0 \quad \text{with} \quad \mathbf{J} = \rho(\mathbf{v} - \mathbf{w}). \quad (7)$$

Furthermore, the general total outward flux \mathbf{J}^ψ can be written as the sum of a convective (mass-related) part $\rho\psi(\mathbf{v} - \mathbf{w})$ and a conductive part² $\mathbf{J}_{\text{cond}}^\psi$. Clearly, if domain Ω is a body, the convective part vanishes because $\mathbf{v} = \mathbf{w}$.

Applying Reynolds transport theorem and the divergence theorem to Eq. (5), we obtain the local form of the generic balance equation [5]:

$$\frac{\partial \rho \psi}{\partial t} + \nabla \cdot \left(\mathbf{v} \rho \psi + \mathbf{J}_{\text{cond}}^\psi \right) = \Pi^\psi + \Sigma^\psi. \quad (8)$$

The specific balances of mass, momentum, total and internal energy, etc., follow directly by inserting the according expressions for ψ , $\mathbf{J}_{\text{cond}}^\psi$, Π^ψ , and Σ^ψ ; cf. [1].

3.2. Mesoscopic space and distribution function

Complex materials require more variables in order to describe the material behavior effectively (e.g., internal spins for micro-polar medias or damage parameters for cracked materials). Then, the question arises how these additional quantities can be included in the classical continuum-mechanical framework

²The mass flux has per definition no conductive part, $\mathbf{J}_{\text{cond}}^1 = 0$.

of kinematical, balance, and constitutive equations. For this reason, different approaches have been established; cf. [1]. One possibility is the extension of the state space by means of extra fields, so-called internal variables. They have a specific physical background and require additional equations (e.g., rate equations), which in general must be defined ad hoc.

The mesoscopic concept is different and in some sense easier. An extended domain $(\mathbf{m}, \mathbf{x}, t)$ is introduced, where $\mathbf{m} \in \mathcal{M}$ identifies the mesoscopic variables spanning the mesoscopic manifold \mathcal{M} . This extended configurational space is called the *mesoscopic space*; cf. [1]:

$$(\mathbf{m}, \mathbf{x}, t) \in \mathcal{M} \times \mathbb{R}^3 \times \mathbb{R}, \quad (9)$$

on which now the usual fields, such as mass density $\tilde{\varrho} := \varrho(\mathbf{m}, \mathbf{x}, t)$, material velocity $\tilde{\mathbf{v}} := \mathbf{v}(\mathbf{m}, \mathbf{x}, t)$, internal energy density $\tilde{e} := e(\mathbf{m}, \mathbf{x}, t)$, stress tensor $\tilde{\boldsymbol{\sigma}} := \boldsymbol{\sigma}(\mathbf{m}, \mathbf{x}, t)$, etc., have to be redefined.³ Consequently, the balances of mass, momentum, and energy also need to be reformulated on the mesoscopic space.

Note that the classical balance equations defined on the space–time domain (\mathbf{x}, t) do still apply. However, the position vectors \mathbf{x} now label a volume element with certain mesoscopic variables. In general, the particles of a volume associated with (\mathbf{x}, t) do not have the same values of the mesoscopic variable \mathbf{m} . Thus, a statistical element needs to be introduced that accounts for the distribution of \mathbf{m} at each time t and position \mathbf{x} – this is the so-called *mesoscopic distribution function* (MDF), $\tilde{d} := d(\mathbf{m}, \mathbf{x}, t)$. The physical meaning of the MDF in a volume element with the total number of $N(\mathbf{x}, t)$ particles is as follows: Let $\{N(\mathbf{m}, \mathbf{x}, t)\} \subset \{N(\mathbf{x}, t)\}$ be a subset, identifying all particles with the same value of \mathbf{m} . Then \tilde{d} defines the fraction of the \mathbf{m} -valued particles at (\mathbf{x}, t) as follows:

$$\tilde{d} := \frac{N(\mathbf{m}, \mathbf{x}, t)}{N(\mathbf{x}, t)} = \frac{\tilde{N}}{N}. \quad (10)$$

Summarizing over all \tilde{N} results in N , the following normalization holds:

$$N = \int_{\mathcal{M}} \tilde{N} \, d\mathbf{m} \quad \Rightarrow \quad \int_{\mathcal{M}} \tilde{d} \, d\mathbf{m} = \frac{1}{N} \int_{\mathcal{M}} \tilde{N} \, d\mathbf{m} = 1. \quad (11)$$

Note that \tilde{d} has no analog in the classical macroscopic description, so the mesoscopic concept handles more information than the conventional macro-

³For distinguishing these fields from the usual, macroscopic ones and to omit the arguments in the remaining of the text, we have added a tilde to the symbols when we speak of mesoscopic quantities.

scopic one. Furthermore, the MDF in Eq. (10) can be used to define the fields of mass density, momentum, total energy, etc., on the mesoscopic space. In particular, the mesoscopic mass density reads

$$\tilde{\varrho} = \tilde{d}\varrho(\mathbf{x}, t) = \frac{\tilde{N}}{N} \varrho(\mathbf{x}, t) \quad (12)$$

and describes the mass density of all particles in a volume element for which the value of the mesoscopic variable is \mathbf{m} . Obviously, the macroscopic mass density $\varrho(\mathbf{x}, t)$ can be recovered from Eq. (12) by integration over the mesoscopic space:

$$\varrho(\mathbf{x}, t) = \int_{\mathcal{M}} \tilde{\varrho} \, d\mathbf{m}. \quad (13)$$

It is worth mentioning that Eq. (13) represents a continuous counterpart to the well-known relation of classical mixture theory, $\rho = \sum_{\nu} \rho_{\nu}$. Here the mass density results from the sum of the partial mass densities ρ_{ν} of the constituents ν .

In the case of the porous material model under consideration, we want to investigate a volume element (VE) containing an ensemble of spherical shells with pores of different radii. Hence, the mesoscopic variables \mathbf{m} can be reduced to the scalar pore radius⁴ a . The number of shells with the same pore radius is $\tilde{N}_P := N_P(a, \mathbf{x}, t)$. Moreover, we shall suppose that the maximum pore radius is bounded by half of the characteristic length of the volume element, $l_{VE} = \sqrt[3]{dV}$. In the applications we have in mind, this will be in the range of a few hundred microns. On the other hand, pores may shrink to infinitesimal size, $a \rightarrow 0$, and we can write $a \in \mathcal{M}$ with $\mathcal{M} \equiv (0, l_{VE}/2]$. Consequently, the total number of shells within a volume element, $N_P(\mathbf{x}, t)$, results from \tilde{N}_P by integration, cf. Eq. (11)₁:

$$N_P(\mathbf{x}, t) = \int_0^{l_{VE}/2} \tilde{N}_P \, da. \quad (14)$$

Further, the mesoscopic mass density results as the product of the macroscopic mass density $\varrho(\mathbf{x}, t)$ and the MDF in Eq. (12). The latter is now actually a pore size distribution function, $\tilde{d} := \tilde{N}_P/N_P(\mathbf{x}, t)$. In turn, like other macroscopic quantities, the mass density $\varrho(\mathbf{x}, t)$ can be recovered from the mesoscopic

⁴The sole use of the scalar mesoscopic variable a presumes a dependence between the different radii $a(t)$ and $b(t)$ within the spherical shell ensemble. This is invoked by volume-preserving deformations of the matrix material as described in Section 2. A more general case could be found introducing a vectorial mesoscopic variable $\mathbf{m} = (a, b)$.

quantity $\tilde{\varrho}$ by integration over the mesoscopic space; this basically corresponds to a sum over all spherical shells:

$$\varrho(\mathbf{x}, t) = \int_0^{l_{\text{VE}}/2} \tilde{\varrho} \, da \quad \text{with} \quad \tilde{\varrho} = \tilde{d}\varrho(\mathbf{x}, t). \quad (15)$$

3.3. Mesoscopic balance equations

From a mathematical point of view, the mesoscopic balance equations differ from the macroscopic ones only in their domain, which is enlarged by the mesoscopic variables, i.e., the domain of integration is now $\Omega \times \mathcal{M}$. Therefore, derivatives with respect to the variables $(\mathbf{m}, \mathbf{x}, t)$ appear in the balances, and the flux of Ψ can be written as $\tilde{\mathbf{J}}^\Psi = \tilde{\mathbf{J}}^{\Psi, \Omega} \cup \tilde{\mathbf{J}}^{\Psi, \mathcal{M}}$, i.e., a flux per spatial surface and per the manifold \mathcal{M} , respectively. Following Muschik et al. in [2], the *local form of the mesoscopic generic balance* reads:

$$\frac{\partial}{\partial t} \tilde{\rho} \tilde{\psi} + \nabla_x \cdot \left[\tilde{\mathbf{v}} \tilde{\rho} \tilde{\psi} - \tilde{\mathbf{J}}_{\text{cond}}^{\Psi, \Omega} \right] + \nabla_m \cdot \left[\tilde{\mathbf{u}} \tilde{\rho} \tilde{\psi} - \tilde{\mathbf{J}}_{\text{cond}}^{\Psi, \mathcal{M}} \right] = \tilde{\Pi} \tilde{\psi} + \tilde{\Sigma} \tilde{\psi}, \quad (16)$$

where $\tilde{\mathbf{J}}_{\text{cond}}^{\Psi, \Omega}$ and $\tilde{\mathbf{J}}_{\text{cond}}^{\Psi, \mathcal{M}}$ are the *conductive* parts of the fluxes (see comment on Eq. (7)). The analog to the material velocity $\tilde{\mathbf{v}}$ is the *velocity of mesoscopic change* $\tilde{\mathbf{u}} := \mathbf{u}(\mathbf{m}, \mathbf{x}, t)$, which is defined by the following mapping:

$$(\mathbf{m}, \mathbf{x}, t) \longmapsto (\mathbf{m} + \tilde{\mathbf{u}} dt, \mathbf{x} + \tilde{\mathbf{v}} dt, t + dt). \quad (17)$$

The symbols t and $(t + dt)$ denote two instances of one particle at \mathbf{x} . In more detail, the local mesoscopic balance for *mass* $\tilde{\varrho}$, *linear momentum* $\tilde{\mathbf{l}} = \tilde{\varrho} \tilde{\mathbf{v}}$, and *total energy density* $\tilde{e} = \frac{1}{2} \tilde{\varrho} (\tilde{\mathbf{v}}^2 + \tilde{u})$ are:

$$\frac{\partial \tilde{\varrho}}{\partial t} + \nabla_x \cdot (\tilde{\varrho} \tilde{\mathbf{v}}) + \nabla_m \cdot (\tilde{\varrho} \tilde{\mathbf{u}}) = 0, \quad (18)$$

$$\frac{\partial \tilde{\mathbf{l}}}{\partial t} + \nabla_x \cdot (\tilde{\mathbf{v}} \tilde{\mathbf{l}} - \tilde{\boldsymbol{\sigma}}^T) + \nabla_m \cdot (\tilde{\mathbf{u}} \tilde{\mathbf{l}} - \boldsymbol{\zeta}^T) = \tilde{\varrho} \tilde{\mathbf{k}}, \quad (19)$$

$$\frac{\partial \tilde{e}}{\partial t} + \nabla_x \cdot (\tilde{\mathbf{v}} \tilde{e} - \tilde{\boldsymbol{\sigma}}^T \cdot \tilde{\mathbf{v}} + \tilde{\mathbf{q}}) + \nabla_m \cdot (\tilde{\mathbf{u}} \tilde{e} - \boldsymbol{\zeta}^T \cdot \tilde{\mathbf{v}} + \tilde{\boldsymbol{\omega}}) = \tilde{\varrho} \tilde{\mathbf{k}} \cdot \tilde{\mathbf{v}} + \tilde{\varrho} \tilde{r}. \quad (20)$$

Here, $\boldsymbol{\zeta}$ denotes an analog to the stress tensor, the non-convective momentum flux with respect to the mesoscopic variables \mathbf{m} and $\tilde{\mathbf{k}}$ being the sum of all external specific forces. The symbol \tilde{u} stands for the specific internal energy, and \tilde{r} identifies a possible mesoscopic energy supply (i.e., by means of radiation). Furthermore, the mesoscopic heat flux density is $\tilde{\mathbf{q}}$, and $\tilde{\boldsymbol{\omega}}$ represents the corresponding heat flux density on \mathcal{M} .

The mesoscopic balances of spin, angular momentum, and internal energy can be also formulated [2]. Besides, the *mesoscopic balance of entropy* is of no special interest, because the mesoscopic entropy production is not necessarily positive definite.

The MDF defined in Eq. (10) also follows an own balance. For their derivation, we follow again the approach of [2] and insert Eq. (12) into Eq. (18):

$$\frac{\partial}{\partial t} [\tilde{d} \varrho(\mathbf{x}, t)] + \nabla_x \cdot [\varrho(\mathbf{x}, t) \tilde{d} \tilde{\mathbf{v}}] + \nabla_m \cdot [\varrho(\mathbf{x}, t) \tilde{d} \tilde{\mathbf{u}}] = 0. \quad (21)$$

By means of the macroscopic mass balance resulting from Eq. (8), $\frac{\partial \varrho}{\partial t} + \nabla_x \cdot \nu \varrho = 0$, the *balance of the MDF* can be written as

$$\frac{\partial \tilde{d}}{\partial t} + \nabla_x \cdot (\tilde{d} \tilde{\mathbf{v}}) + \nabla_m \cdot (\tilde{d} \tilde{\mathbf{u}}) = -\frac{\tilde{d}}{\varrho} \left[\frac{\partial \varrho}{\partial t} + \tilde{\mathbf{v}} \cdot \nabla_x \varrho \right]. \quad (22)$$

The right-hand side of Eq. (22) may also be written as $-\tilde{d} \frac{d}{dt} (\ln \varrho) / \varrho$ with $\varrho \equiv \varrho(\mathbf{x}, t)$. Thus the macroscopic mass density $\varrho = \varrho(\mathbf{x}, t)$ influences the MDF \tilde{d} , an effect which is often denoted as a “mean-field” effect; cf. [2]. However, the macroscopic balances can be recovered from the mesoscopic ones by replacing the mesoscopic space with the space–time domain (\mathbf{x}, t) . The macroscopic fields result by integrating over \mathcal{M} analogously to Eq. (13):

$$\mathbf{v}(\mathbf{x}, t) := \int_{\mathcal{M}} \tilde{d} \tilde{\mathbf{v}} dm, \quad e(\mathbf{x}, t) := \int_{\mathcal{M}} \tilde{d} \tilde{e} dm, \quad \text{etc.} \quad (23)$$

The balance of the MDF, Eq. (22), requires a material law for the mesoscopic change velocity $\tilde{\mathbf{u}}$. Because of the dependence of $\tilde{\mathbf{u}}$ on the considered complex material property, e.g., the microstructure, here no universal approach exists. Examples for its determination are given in [2] for uniaxial liquid crystals, where the corresponding velocity of mesoscopic change characterizes the orientational change of the so-called microscopic director $\mathbf{n} \in S^2$, which can be derived by means of the spin balance. Another example are microcracks in linear elastic materials; cf. [3, 6]. Here the mesoscopic variables are the crack length l and the crack orientation \mathbf{n} , i.e., $\mathbf{m} = (l, \mathbf{n})$; the velocity of mesoscopic change $\tilde{\mathbf{u}}$ can be found by means of the Rice–Griffith dynamics.

In the case of the porous model considered here, the scalar pore radius a is simply used for \mathbf{m} . Thus the velocity of mesoscopic change is given by \dot{a} and the derivative ∇_m of Eqs. (18)–(20), (22) stands for $\partial/\partial a$.

3.4. Balance of the pore distribution function

Here we specify the mesoscopic approach to the porous material model of Section 2. The crucial variable for the mesoscopic description is given by the mesoscopic pore number \tilde{N}_P or by its normalized counterpart $\tilde{d} = \tilde{N}_P/N_P(t)$; see Eq. (10). Therefore, we formulate the balance equation (22) in terms of \tilde{N}_P ,

$$\frac{\partial \tilde{N}_P}{\partial t} + \nabla_x \cdot (\tilde{N}_P \tilde{\mathbf{v}}) + \frac{\partial}{\partial a} (\tilde{N}_P \dot{a}) = \tilde{\Pi}^{\tilde{N}_P} \quad (\text{balance of mesoscopic pore number}). \quad (24)$$

The right-hand side of Eq. (24) represents a production term referring to pore nucleation and/or coalescence and will be discussed below. In the simplest case of a constant pore number, it holds $\tilde{\Pi}^{\tilde{N}_P} = 0$ and we get a conservation law. The mesoscopic translational velocity $\tilde{\mathbf{v}} := \mathbf{v}(a, t)$ does not depend on pore radius a , i.e., it is identical for all shells and pores. It can be identified with the macroscopic velocity of the volume element, $\tilde{\mathbf{v}} = \mathbf{v}(\mathbf{x}, t)$, because the different pores are embedded in the surrounding material of the porous solid and are not thought to move independently.

In order to derive the balance for the pore distribution function \tilde{d} , we multiply Eq. (24) with $1/N_P$ and apply Eq. (10); a minor calculation results in

$$\frac{\partial \tilde{d}}{\partial t} + \nabla_x \cdot (\tilde{d} \mathbf{v}) + \frac{\partial}{\partial a} (\tilde{d} \dot{a}) = \tilde{\Pi}^{\tilde{N}_P} + \frac{\tilde{d}}{N_P} \left(\frac{\partial N_P}{\partial t} + \mathbf{v} \cdot \nabla_x N_P \right). \quad (25)$$

The bracketed expression of the right-hand side of Eq. (25) denotes the material time derivative $\partial_t N_P + \mathbf{v} \cdot \nabla_x N_P = \mathbf{d}_t N_P = \dot{N}_P$ of the *macroscopic* pore number, i.e., the temporal change of N_P in the volume element noticeable by a co-moving observer. Consequently, *two production terms* occur: (i) The mesoscopic production, $\tilde{\Pi}^{\tilde{N}_P}$, which accounts for sources or sinks of pores with a specific radius a , and (ii) the macroscopic pore number production, $\Pi^{N_P} := \dot{N}_P$, which identifies the total change of N_P in the volume element. Clearly, summing up the different mesoscopic productions over all radii results in the macroscopic quantity \dot{N}_P . Thus Π^{N_P} and $\tilde{\Pi}^{\tilde{N}_P}$ are not independent but it holds according to Eq. (14):

$$\Pi^{N_P} = \int_0^{l_{VE}/2} \tilde{\Pi}^{\tilde{N}_P} da. \quad (26)$$

With these considerations, the *balance of the pore distribution function* can be written in the following compact forms:

$$\frac{\partial \tilde{d}}{\partial t} + \nabla_x \cdot (\tilde{d}\mathbf{v}) + \frac{\partial}{\partial a}(\tilde{d}\dot{a}) = \tilde{\Pi}^{\tilde{N}_P} + \frac{\tilde{d}}{N_P} \Pi^{N_P} \quad (\text{with pore production}), \quad (27)$$

$$\frac{\partial \tilde{d}}{\partial t} + \nabla_x \cdot (\tilde{d}\mathbf{v}) + \frac{\partial}{\partial a}(\tilde{d}\dot{a}) = 0 \quad (\text{without pore production}). \quad (28)$$

The balances of distribution function (22) and of pore distribution function (27) have the same structure except for the mesoscopic production term $\tilde{\Pi}^{\tilde{N}_P}$, which is zero in Eq. (22) due to mass conservation. If both nucleation and coalescence of pores are negligible, no mesoscopic pore production occurs and the total pore number N_P remains constant. Then, Eqs. (27) and (22) are identical with vanishing right-hand sides. In addition, excluding pore production, only a constitutive relation for the *pore expansion velocity* \dot{a} is required to solve Eq. (28). We will provide this in the following.

4. Analysis of oscillating bubbles

By means of the introduced mesoscopic approach, the macroscopic (wanted) fields can be described more precisely, namely, enriched with the microstructural information of the mesoscopic distribution function; cf. Eq. (23). To specify this approach for the porous material model of Section 2, we summarize, at first, the underlying assumptions:

- From the mechanical point of view, the (ESWL-treated) human kidney is a conglomerate of liquid-containing cells in which the hypersonic excitation activates the nucleation and oscillation of bubbles. Here we assume the “soaked tissue” to be a soft solid in which initially very small bubbles are already embedded. The soft solid is modelled as an ensemble of spherical shells, i.e., bubbles of different sizes are surrounded by elastic, isotropic, and incompressible matrix material. The processes of bubble nucleation and coalescence are neglected; Eq. (28) holds.
- The spherical shell ensemble is exposed to externally applied forces that invoke an inhomogeneous stress field $\tilde{\boldsymbol{\sigma}} := \boldsymbol{\sigma}(a, \mathbf{x}, t)$ due to the heterogeneity of the volume element dV with stiffness $\mathbb{C} = \mathbb{C}(a, \mathbf{x}, t)$. Here we assume an *averaged* stress field of the form $\boldsymbol{\sigma} = \tilde{\boldsymbol{\sigma}}$, i.e., all spherical shells “feel” the same loading.⁵

⁵This assumption is established in the field of homogenization as the Reuss approximation [7] and leads to an effective stiffness \mathbb{C}^* representing a lower bound for the heterogeneous material [8].

- The power $\tilde{P} := P(a, \mathbf{x}, t)$ of the external forces acting on *one* spherical shell is completely compensated by the power accompanied with the deformation of the spherical shell and the expansion of the containing bubble. The volume remaining between the spherical shells is presumed to vanish, $V_{\text{rem}} \rightarrow 0$.

4.1. Constitutive model for the bubble velocity

Consider now an ensemble of spherical shells identifiable, e.g., with a volume element dV , and subjected to an external load. We postulate the existence of a free energy function $A(\mathbf{x}, t)$ as a weighted sum of free energy contributions of all spherical shells. Symbol \tilde{A} represents the energy required to deform *one* shell i with bubble radius $a \equiv a^{(i)}$ and with $\tilde{A} := \sum_j \tilde{A}_j^{(i)}$; here the $\tilde{A}_j^{(i)}$ denotes different energy contributions j of shell deformation and bubble expansion. In view of soft tissues *three* forms of energy dominate: (1) elastic energy \tilde{W}^e of the deforming matrix material, (2) kinetic energy \tilde{K} due to bubble expansion, and (3) surface energy \tilde{S} stored in the interface between bubble and matrix.

The external power \tilde{P} put into one spherical shell is a function of the remotely applied pressure $p(t)$ and completely compensated by the rate of free energy $d_t \tilde{A} = d_t \sum_j \tilde{A}_j^{(i)}$, i.e.,

$$\tilde{P} = p(t) \cdot \frac{d\tilde{V}_{\text{shell}}}{dt} = \frac{d\tilde{A}}{dt} = \frac{d}{dt} (\tilde{W}^e + \tilde{K} + \tilde{S}). \quad (29)$$

With a specified right-hand side and with initial values a_0 and b_0 , Eq. (29) represents a differential equation for $a(t)$ in one spherical shell. Solving this equation for different initial conditions yields a constitutive relation for the mesoscopic bubble velocity $\dot{a} \equiv \dot{a}(a, t)$. Let us now consider the energy contributions in detail.

4.1.1. Elastic energy The elastic response of a soft tissue may simply be described by a *Neo-Hookean material* with the strain energy density w^e :

$$w^e = \frac{\mu}{2} (\mathbf{B} - 3) = \frac{\mu}{2} (\lambda_1^2 + \lambda_2^2 + \lambda_3^2 - 3), \quad (\mu : \text{shear modulus}). \quad (30)$$

Here $\mathbf{B} = \mathbf{F}\mathbf{F}^T$ stands for the left Cauchy Green tensor and \mathbf{F} identifies the deformation gradient. Furthermore, $\lambda_{1,2,3}$ represent the principle stretches. Note that the energy formalism of an elastic material law, such as Eq. (30), is known as a *hyperelastic material law*. In particular, Eq. (30) characterizes a special case of so-called Mooney–Rivlin materials suitable to describe

materials with a large elastic range and commonly applied to biological soft tissue [9, 10].

Exploiting the spherical shell geometry and the matrix incompressibility constraint it holds for some radius r and with $\lambda = r/r_0$; cf. Figure 2:

$$\mathbf{F} = \begin{bmatrix} \lambda & 0 & 0 \\ 0 & \lambda & 0 \\ 0 & 0 & 1/\lambda^2 \end{bmatrix} \Rightarrow \mathbf{B} = \begin{bmatrix} \lambda^2 & 0 & 0 \\ 0 & \lambda^2 & 0 \\ 0 & 0 & \lambda^{-4} \end{bmatrix}. \quad (31)$$

The elastic energy of one spherical shell then follows by integration,

$$\begin{aligned} \tilde{W}^e &:= W^e(a) = \int_a^b w^e(r) 4\pi r^2 \, dr \\ &= \frac{\mu}{2} \int_a^b \left[2 \left(\frac{r}{r_0} \right)^2 + \left(\frac{r_0}{r} \right)^4 - 3 \right] 4\pi r^2 \, dr \\ &= 2\pi \mu \left(a_0^3 - b_0^3 - \frac{a_0}{a} (2a^3 - a_0^3) + \frac{b_0}{b} (2b^3 - b_0^3) \right). \end{aligned} \quad (32)$$

The total elastic energy of the complete spherical shell ensemble can be calculated by the “weighted sum” over the individual spherical shells using the mesoscopic distribution function (28). It reads:

$$W^e(\mathbf{x}, t) = \int_0^{l_{VE}/2} \tilde{d} \tilde{W}^e \, da. \quad (33)$$

4.1.2. Kinetic energy By means of the radial component of spatial velocity, Eq. (4), one can also calculate the kinetic energy of an expanding spherical shell and – analogously to Eq. (33) – the kinetic energy of the total porous ensemble:

$$\tilde{K} := K(a, \dot{a}) = \int_a^b \frac{1}{2} \varrho_0 v_r^2 4\pi r^2 \, dr = 2\pi \varrho_0 a^4 \left(\frac{1}{a} - \frac{1}{b} \right) \dot{a}^2, \quad (34)$$

$$K(\mathbf{x}, t) = \int_0^{l_{VE}/2} \tilde{d} \tilde{K} \, da \quad \text{with} \quad b = b(a). \quad (35)$$

Here, ϱ_0 denotes the mass density of the matrix material, which is constant because of the assumption of incompressibility.

4.1.3. Surface energy The surface energy \tilde{S} in the interface of a bubble with radius a and with surface tension γ (of unit [N/m]) as well as the according total surface energy of the whole ensemble are

$$\tilde{S} := S(a) = 4\pi a^2 \gamma \quad \text{and} \quad S(\mathbf{x}, t) = \int_0^{l_{VE}/2} \tilde{d}\tilde{S} \, da. \quad (36)$$

4.1.4. External power The external power resulting from an applied pressure history $p(t)$ and the deformation of one spherical shell is given by Eq. (29). With the kinematics of Section 2.2, it holds that $\tilde{P} = p(t) \cdot \mathbf{d}_t \left(\frac{4}{3}\pi (b_0^3 - a_0^3 + a^3) \right)$. Consequently, one can write for \tilde{P} and for the macroscopic power P consumed by the whole spherical shell ensemble

$$\tilde{P} = p(t) \cdot 4\pi a^2 \dot{a} \quad \text{and} \quad P(\mathbf{x}, t) = \int_0^{l_{VE}/2} \tilde{d}\tilde{P} \, da. \quad (37)$$

4.1.5. Governing differential equation Combining Eq. (29) with the Eqs. (32), (34), (36)₁, and (37)₁ results in an ordinary differential equation for radius $a(t)$,

$$\begin{aligned} 0 &= \tilde{P} - \frac{d}{dt} (\tilde{W}^e + \tilde{K} + \tilde{S}) \\ &= p(t) \cdot a^2 \dot{a} - \mu a^2 \left[\frac{b_0}{2b} \left(\frac{b_0^3}{b^3} + 4 \right) - \frac{a_0}{2a} \left(\frac{a_0^3}{a^3} + 4 \right) \right] \dot{a} - 2a\gamma \dot{a} \\ &\quad - \frac{\rho_0}{2} \left[2\ddot{a}\dot{a}a^3 + 3\dot{a}^3 a^2 - \frac{a^3}{b} \left(2\ddot{a}\dot{a}a + 4\dot{a}^3 - \frac{a^3 \dot{a}^3}{b^3} \right) \right], \end{aligned} \quad (38)$$

with $b = (b_0^3 - a_0^3 + a^3)^{1/3}$ according to Eq. (3)₂. Equation (38) can be solved (numerically) for *one* shell (i) of radius $a(t)$ and with the initial geometry $a_0 = a(t = 0)$ and $b_0 = b(t = 0)$. The exploitation of a spherical shell ensemble (consisting of shells with different radii) requires the numerical solution of Eq. (38) for all i initial geometries. Once \dot{a} has been found to be the resulting velocity of bubbles of size a , the balance of the distribution function, Eq. (28), can be solved.

4.2. Bubble dynamics

In an attempt to illustrate the capability of the constitutive model, we investigate the temporal development of bubbles with different initial radii. The

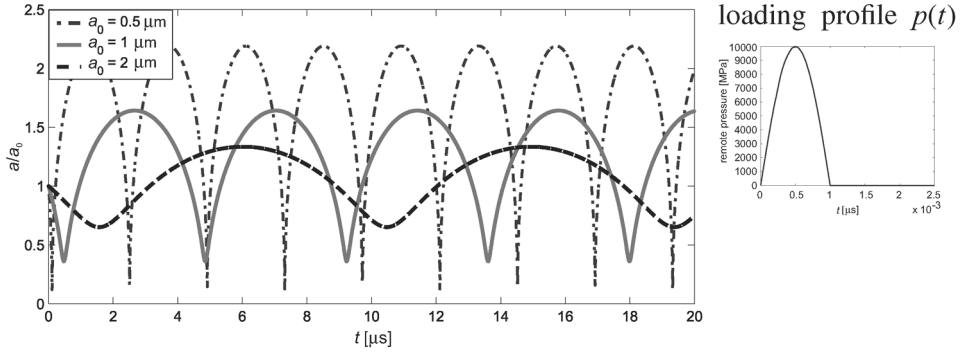


Figure 4. Oscillation of bubbles with different initial radii in a soft elastic media enforced by a pressure impulse of $p_0 = -1$ MPa within $t_p = 1$ ns.

power of external forces follows from a sudden pressure impulse as typical in an ESWL treatment. A pressure \bar{p} with magnitude of 1 MPa is applied within 1 ns, and is set to zero afterwards. It follows from Eq. (38)

$$\ddot{a} = \left\{ \rho_0^{-1} \left[\bar{p}a^2 - 2a\gamma - \mu a^2 \left(\frac{b_0}{2b} \left(\frac{b_0^3}{b^3} + 4 \right) - \frac{a_0}{2a} \left(\frac{a_0^3}{a^3} + 4 \right) \right) \right] - \dot{a}^2 \left(\frac{3a^2}{2} - \frac{2a^3}{b} + \frac{a^6}{2b^4} \right) \right\} \times \left(a^3 - \frac{a^4}{b} \right)^{-1}. \quad (39)$$

The elastic matrix material surrounding the bubbles is a soft tissue with material data $\mu = 500$ Pa, $\gamma = 1$ N/m, and $\rho = 1050$ kg/m³. Figure 4 displays the evolution of radius $a(t)$ for bubbles (or pores) with initial radius $a_0 = \{0.5, 1.0, 2.0\}$ μm. Due to the incompressibility of the matrix medium, all volume changes are a consequence of pore evolution. Therefore, the pressure impulse forces the pores to close, i.e., $a \rightarrow 0$. After the impulse has passed, the pores expand again but the attained maximal pore radius a_{\max} is much bigger than the initial radius a_0 because of elasticity and inertia effects. This process is similar to the cavitation process observed in fluids that are subjected to (high-intensity) pressure waves [11]. It is interesting to note that the ratio of a_{\max}/a_0 increases the smaller the initial pore is whereas the periodic time of one oscillation decreases for a smaller initial pore radius. Equation (39) does not account for any dissipation. Thus, the process of growth and compression continues periodically. In all displayed cases, the initial porosity of the material is $f_{V0} = 10^{-6}$. Raising this value (significantly) increases amplitude and frequency (a little); a lower value of f_{V0} has de facto no effect.

Finally, we want to emphasize that our model is essentially based on the volumetric incompressibility of the material surrounding the pore. This was done to ease the derivation of a constitutive model, but it is also justified by the particular materials under consideration. Most bio-materials are (almost) incompressible.

4.3. Bubble distribution and damage parameter

4.3.1. Evolution of the mesoscopic distribution function Let us now consider an ensemble of different bubbles. Their number and size are described by the mesoscopic distribution function, Eq. (28). The external power acting on the ensemble of (unit) volume, $dV(\mathbf{x}, t)$, is applied by a sudden pressure impulse as described in Section 4.2. The problem of interest now is how does the bubble distribution $\tilde{d}(t)$ change in time.

Clearly, different frequencies and amplitudes of bubble oscillations result in different bubble distributions for every instance. For simplicity, we assume the initial bubble distribution to be an equipartition, i.e., the number of bubbles is the same for all radii $a \in (0, a_{0 \max}]$. Exemplarily, we display in Figure 5 the analysis of an ensemble of three bubbles with maximal initial radius of $a_{0 \max} = 1.5 \mu\text{m}$.

Subjected to the loading impulse, all bubbles compress. From the analysis of Section 4.2, we know that bubbles with small initial size are less inert and shrink faster than their bigger companions. Consequently, the change of distribution function \tilde{d} is not symmetric. After a few microseconds, the bubbles expand and grow – with different velocities – over their original

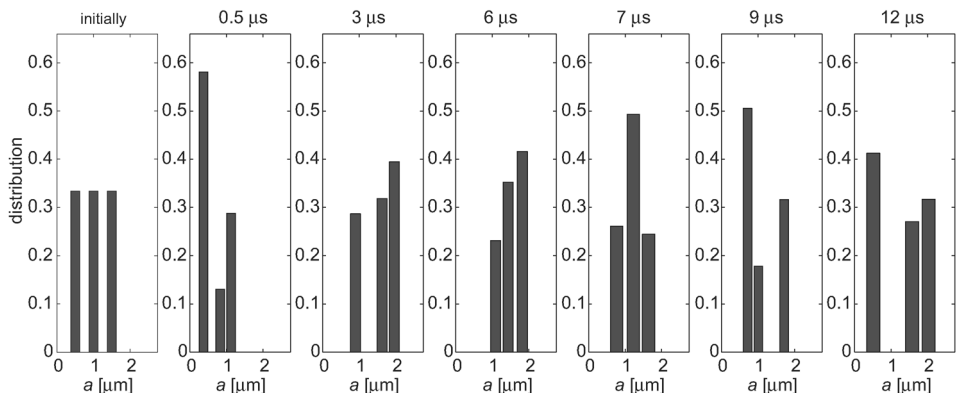


Figure 5. Distribution of an ensemble of three bubbles with $a_0 = \{0.5, 1.0, 1.5\} \mu\text{m}$ and with initially equal distribution at different instances after loading with a pressure impulse of $\bar{p} = 1 \text{ MPa}$.

size. Then the process of growth and compression continues periodically and undamped. Therefore, no stable or final state of bubble distribution will be attained, and Figure 4 just shows some “snapshots” of the distribution. To obtain a final state of distribution function (28), a dissipative term needs to be added to the constitutive law (39). We will follow such an approach in a subsequent paper.

4.3.2. Damage parameters I. General remarks In the introduction, we briefly addressed the adverse effects accompanying the hypersonic radiation of soft tissue. Health professionals are increasingly interested in the prediction of these tissue injuries or, in other words, in the prediction of material damage. However, the microscopic origin of damage in an ESWL treatment is an open question. The existing arguments are multifaceted, cf. [12], but it is certain that hypersonic waves initiate *two* effects: (1) the cavitation of bubbles and (2) different tissue motions. Bubble cavitation results in dilatation of the enclosing tissue, which eventually leads to damage. On the other hand, the cavitated bubbles tend to collapse and induce micro-jets, an alternative reasonable damage source. In contrast, the different tissue motion coming from various wave strengths of the inhomogeneous tissue may result in cell shearing and lysis, which also represent a possible damage source.

All these phenomena identify realistic scenarios, and up to now it has been unclear which are the driving effects (probably it is a combination of several effects). But let us assume for a moment that the origin of damage is clarified; then the question about the quantification of damage arises, which is closely related to the definition of a *damage parameter*.

In what follows, we propose two definitions of a damage parameter related to cavitation. The first one, a measure of a representative bubble radius, presumes the dilatation of the tissue material during the cavitation process to be the driving damaging effect. The second definition considers the energy application rate and assumes the resulting total dissipated power to be a measure of damage.

4.3.3. Damage parameters II. Critical bubble radius Let damage in the material be characterized by a material-dependent macroscopic parameter $D(\mathbf{x}, t)$. This parameter indicates the local temporal evolution of irreversible material changes and is, by nature, monotone and continues in time. For the class of materials considered here, we suggest, at first, that the material is irreversibly strained and damage happens when a critical bubble radius a_{crit} is exceeded. In consequence, a bubble oscillation with constant amplitude (and with radii of $a > a_{\text{crit}}$) as described above is impossible because of

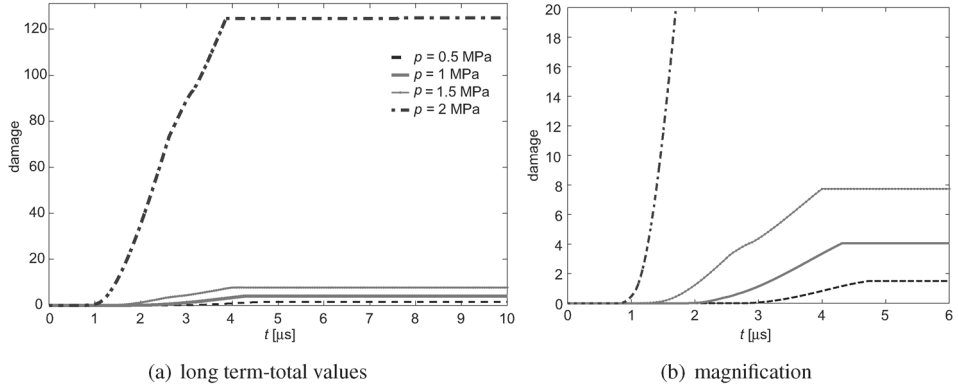


Figure 6 Evolution of damage parameter $D(\mathbf{x}, t)$ at differently loaded volume elements.

the dissipative character of the damaging process. Instead, only the currently occurred maximal radius of *every bubble*,

$$\tilde{q} := q(a, \mathbf{x}, t) = \max_{0 \leq \tau \leq t} a(\mathbf{x}, \tau), \quad (40)$$

can induce damage; subsequent oscillations are not of interest. Thus we suggest

$$D(\mathbf{x}, t) = \int_{a_{\text{crit}}}^{l_{\text{VE}}/2} \tilde{\eta} \tilde{d} \tilde{q} da \quad (41)$$

with the cut-off function

$$\tilde{\eta} := \eta(a, \mathbf{x}, t) = \begin{cases} c & \text{if } \tilde{q} \geq a_{\text{crit}} \text{ and } a(\mathbf{x}, t) = \tilde{q} \\ 0 & \text{otherwise.} \end{cases} \quad (42)$$

In Eq. (42), c is a positive constant that can be used to normalize the damage parameter in Eq. (41) but is set to one for now. Figure 6 illustrates the damage evolution according to Eq. (41) for the bubble ensemble of Section 4.3.1, now loaded with four different pressure magnitudes $\bar{p} = \{0.5, 1.0, 1.5, 2\}$ MPa. The critical radius is set to be $a_{\text{crit}} = \max(a_0)$. At the beginning (during compression) no damage occurs, then, depending on the bubble oscillation's amplitude, the damage grows. Because with Eq. (40), bubble oscillation is only considered to damage the material once a steady state is reached. Solely a next pressure impulse would raise the amount of damage again. This is what actually happens in an ESWL treatment where several (thousands of) shocks are applied and damage accumulate. What is remarkable is the big difference

in damage at different pressure magnitudes; therefore, Figure 6 displays the results in two resolutions.

4.3.4. Damage parameters III. Total dissipated power Because of the lack of knowledge about the exact micro-physical mechanisms during the ESWL radiation process at second, a more empirical approach for $D(\mathbf{x}, t)$ is suggested. This is done by means of an energetic criterion based on the assumption that the complete (i.e., macroscopic) power of deformation applied to a spherical shell ensemble, $P(\mathbf{x}, t)$, can be decomposed into a reversible and a dissipated part, $P^{\text{rev}} = P^{\text{rev}}(\mathbf{x}, t)$ and $P^{\text{diss}} = P^{\text{diss}}(\mathbf{x}, t)$, respectively. The latter is considered to be the power of material damage,

$$P^{\text{rev}} + P^{\text{diss}} = \frac{d}{dt} (W^e + K + S), \quad (43)$$

where the expressions of the right hand-side are given by Eqs. (33), (35), and (36)₂. With a *dissipation coefficient* $\alpha \in [0, 1]$, we decompose

$$P^{\text{rev}} = (1 - \alpha) \frac{d}{dt} (W^e + K + S) \quad \text{and} \quad P^{\text{diss}} = \alpha \frac{d}{dt} (W^e + K + S). \quad (44)$$

Note that $\alpha = 0$ represents a reversible process (as displayed in Figure 4), whereas $\alpha = 1$ stands for total dissipation. By means of the mesoscopic background of Paragraph 4.1, we write⁶

$$P^{\text{diss}} = \alpha \frac{d}{dt} \int_{a_0}^{l_{\text{VE}}/2} \tilde{d} (\tilde{W}^e + \tilde{K} + \tilde{S}) da, \quad (45)$$

and we define the total amount of dissipated energy to be the damage parameter

$$\begin{aligned} D(\mathbf{x}, t) &= \alpha \int_0^t \eta(a, \mathbf{x}, t) P^{\text{diss}}(\tau) d\tau \\ &= \alpha \int_{a_0}^{l_{\text{VE}}/2} \eta(a, \mathbf{x}, t) \tilde{d} (\tilde{W}^e + \tilde{K} + \tilde{S}) da. \end{aligned} \quad (46)$$

Function $\eta(a, \mathbf{x}, t)$ accounts for the irreversibility of the damaging process and is defined by Eq. (42). Now Eq. (46) can be calculated using the constitutive relations of the foregoing paragraphs. Hence, parameter $D(\mathbf{x}, t)$ results as a \tilde{d} -weighted average of the mesoscopic energy contributions, $\tilde{W}^e + \tilde{K} + \tilde{S}$.

⁶It is worth mentioning that Eq. (45) is not equal to $P^{\text{diss}} = \int \tilde{d} \cdot \tilde{p}^{\text{diss}} da$ with $\tilde{p}^{\text{diss}} = \alpha \cdot d_t(\tilde{W}^e + \tilde{K} + \tilde{S})$, because of the product rule.

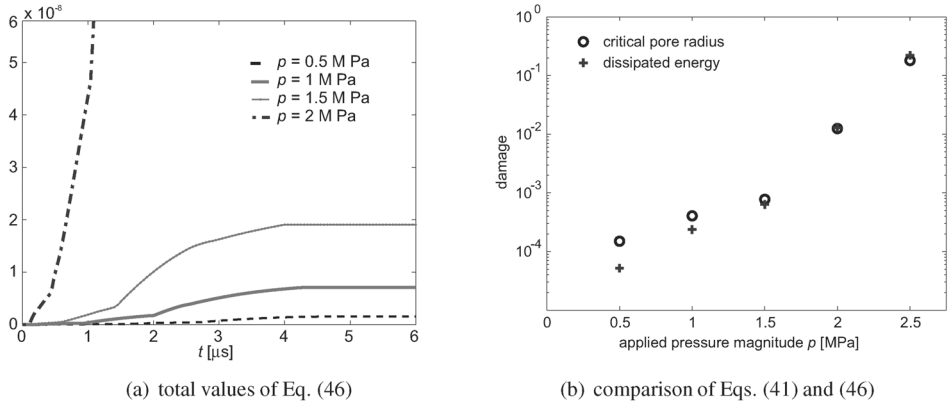


Figure 7. Evolution of damage parameter (46) at differently loaded volume elements and comparison of damage parameters (41) and (46) for raising pressure amplitudes.

Figure 7a illustrates the temporal evolution of damage according to Eq. (46) and (arbitrarily chosen) values of $\alpha = 0.1$, $c = 1$. Note that, although this damage parameter has no direct microscopic meaning and although the absolute values are different, the qualitative prediction of damage is very similar to the parameter of Eq. (41). In particular, the long-term evolution looks the same as in Figure 6a. Therefore, only the magnified equivalent to Figure 6b is plotted here, where we see that damage is measured with Eq. (46) directly from the beginning of bubble growth (and not only after reaching a critical radius). Furthermore, Figure 7b illustrates the growth of damage with raising pressure load in a logarithmic scale. For this plot, the damage parameters of Eqs. (41) and (46) are scaled (choosing constant c in Eq. [42] appropriately). However, it is remarkable that both parameters clearly indicate the same exponential growth of damage with raising load.

5. Conclusions and outlook

In this text, we have established the theoretical framework for a mesoscopic description of pore growth in general continua. The central idea was the introduction of a pore distribution function, \tilde{d} , characterizing the fraction of (spherically assumed) pores of radius a in the considered volume element. Moreover, we derived balance equations, Eqs. (27) and (28); thus, \tilde{d} is predictable by means of initial and boundary conditions. In this way, the wanted macroscopic fields, such as ρ , \mathbf{v} , and e , can be described more precisely including the micro-structural information from the distribution function and the mesoscopic fields. This was done here exemplarily for a porous elastic material with properties of soft biological tissue. A major advantage of the mesoscopic

description is the direct derivation of parameters measuring the damage in a material element as a macroscopic effect but including microstructural information. We have suggested two differently motivated damage parameters, and we point out that both predict exponential growth of damage with raising load.

However, various questions and tasks are open or under current investigation. As it would be interesting to study the behavior of pores in a dissipative material, we will focus on this subject in a subsequent paper. Furthermore, investigations of suitable production terms and an extension of the simulations to pore coalescence is planned for future studies. Finally, questions of the applicability of this model to a real-life model, e.g., in a finite element analysis of a biological structure as in [13], and of its consequences on classical material laws arise.

Acknowledgements

The authors thank W. Muschik, C. Papenfuss (Berlin), and P. Ván (Budapest) for friendly and stimulating discussions. The initial idea of this paper was conceived while the first author held a visiting faculty position in M. Ortiz's group at California Institute of Technology. We would like to thank M. Ortiz for his kind hospitality.

References

- [1] Muschik, W., Papenfuss, C., Ehrentraut, H., A sketch of continuum thermodynamics, *J. Non-Newton Fluid*, 96 (2001), 255–290.
- [2] Muschik, W., Papenfuss, C., Ehrentraut, H., Mesoscopic theory of liquid crystals, *J. Non-Equilib. Thermodyn.*, 29 (2004), 75–106.
- [3] Ván, P., Papenfuss, C., Muschik, W., Griffith cracks in the mesoscopic microcrack theory, *J. Phys. A*, 37 (2004), 5315–5328.
- [4] Bailey, M., Crum, L., Sapozhnikov, O., Evan, A., McAteer, J., Cleveland, R., Colonius, T., Cavitation in shock wave lithotripsy, in: *Proceedings of the 5th International Symposium on Cavitation (CAV2003)*, pp. 1–12, November 1–4, Osaka, Japan, 2003.
- [5] Müller, I., *Thermodynamics*, Pitman Advanced Publishing Program, p. 52, Boston, 2001.
- [6] Papenfuss, C., Ván, P., Muschik, W., Mesoscopic theory of microcracks, *Arch. Mech.*, 55 (2003), 459–477.
- [7] Reuss, A., Berechnung der Fließgrenze von Mischkristallen auf Grund der Plastizitätsbedingungen für Einkristalle, *Z. Angew. Math. Mech.*, 9 (1929), 49–58.
- [8] Gross, D., Seelig, T., *Fracture Mechanics*, pp. 244, 264, Springer-Verlag, Berlin, 2006.
- [9] Treloar, L.R.G., *The Physics of Rubber Elasticity*, 3rd ed., ch. 4, pp. 65–67 and ch. 10, pp. 214–218, Clarendon Press, Oxford, 1975.

- [10] Fung, Y.C., *Biomechanics, Mechanical Properties of Living Tissues*, 2nd ed., ch. 7, pp. 269–320, Springer-Verlag, New York, 1993.
- [11] Howle, L., Schaefer, D.G., Shearer, M., Zhong, P., *Lithotripsy: The treatment of kidney stones with shock waves*, *SIAM Rev.*, 40 (1998), 356–371.
- [12] Lokhandwalla, M., *Damage Mechanisms in Shock Wave Lithotripsy*, ch. 1, pp. 2–4, PhD thesis, California Institute of Technology, Pasadena, 2001.
- [13] Weinberg, K., Ortiz, M., *Shock wave induced damage in kidney tissue*. *Comp. Mater. Sci.*, 32 (2005), 588–593.

Paper received: 2007-04-11

Paper accepted: 2007-06-22